Rotating Bose-Einstein condensate stars at finite temperature

P. S. Aswathi, P. S. Keerthi, O. P. Jyothilakshmi⦿, Lakshmi J. Naik⦿, and V. Sreekanth⦿[*]

Department of Sciences, Amrita School of Physical Sciences,
Amrita Vishwa Vidyapeetham, Coimbatore 641112, India

We study the effect of temperature on the global properties of static and slowly rotating self-gravitating Bose-Einstein condensate (BEC) stars within general relativity. We employ a recently developed temperature-dependent BEC equation of state (EOS) to describe the stellar matter by assuming that the condensate can be described by a nonrelativistic EOS. Stellar profiles are obtained using general relativistic Hartle-Thorne slow rotation approximation equations. We find that with increasing temperatures mass-radius values are found to be decreasing for the static and rotating cases, though the presence of temperature supports high mass values at lower central densities. Countering effects of rotation and temperature on the BEC stellar structure are analyzed and quantified. We report that the inclusion of temperature has a significant effect on the rotating stellar profiles but a negligible effect on the maximum mass, as in the case of a static system. We also study the effect of EOS parameters—boson mass and strength of the self-interaction on global properties of static and rotating BEC stars—in the presence of temperature.

I. INTRODUCTION

The assumption that fundamental scalar fields exist in nature is supported by the detection of the scalar particle Higgs' boson at the Large Hadron Collider, CERN [1,2]. Such scalar fields bound together by their self-generated gravitational interaction can form compact astrophysical objects known as boson stars (see Refs. [3–6] for comprehensive reviews on this topic). It is well known that the scalar fields represent identical bosonic particles that can occupy the same quantum ground state at very low temperatures, forming a Bose-Einstein condensate (BEC). The BEC state, which was predicted by Bose and Einstein, was first experimentally realized by confining ultracold gas of rubidium atoms in a magnetic trap (see Refs. [7,8] for reviews on BECs). Experiments on such trapped dilute Bose gases suggest a phase transition of atoms to the Bose condensed phase, with the particles occupying a coherent state [9–11]. Similarly, a coherent massive object such as boson star can also be realized within astrophysical scales formed of BECs, confined by the self-generated gravitational interaction of bosonic particles. Further, the analysis of Ref. [12] with intense off-resonant laser beams also suggests the possibility of mimicking such BECs bound by gravity in the laboratory.

The self-gravitating compact objects formed with BECs, called BEC stars, have attracted a lot of interest from the research community recently [13–21]. Gravitationally bounded BECs are also considered to be possible candidates of dark matter, which represents a significant amount of the total matter in the Universe and several astrophysical and cosmological studies in this direction have been carried out [22–32]. Bose condensates are also proposed to exist in the interior of neutron stars amidst fermions and these possibilities are studied in detail [33]. Neutron stars with BEC matter are viable because of the fact that neutrons in the star can exist in the superfluid phase, with the particles being treated as composite bosons through Cooper pair formation [34]. In the present work, we concentrate on BEC stars for the analysis.

The dynamics of a self-gravitating BEC at zero temperature is described by the Gross-Pitaevskii (GP) equation [35,36] coupled with the Poisson equation in Newtonian approximation. There are several studies of astrophysical implications of BECs using Newtonian analysis [13–20]. For example, in Ref. [14], the authors study the structure and stability of a self-gravitating BEC system with short-range interactions, and obtained an approximate analytical expression for the mass-radius relation. These analytical relations were compared with the exact mass-radius relations obtained numerically by solving the equation of hydrostatic equilibrium and a good agreement between the two were found [15]. The analyses conducted in Refs. [14,15] are motivated by the idea that dark matter could be a self-gravitating BEC. In Ref. [22], dark matter is being described as a nonrelativistic Bose-Einstein condensate gas with a polytropic equation of state (EOS). There are also studies involving semirelativistic

[*]v_sreekanth@cb.amrita.edu

123001-1

formalisms, in which the stellar matter is described using a nonrelativistic EOS, while the general relativistic approach is used to obtain the stellar structure configurations [16,17].

The possibility of the existence of rotating BEC stars has also been considered in several works. Rotating boson stars have been studied in Ref. [37] within the Newtonian approximation and their analysis suggests that the non-relativistic rotation can be applied only to smaller bosonic objects. Reference [38] studies cold Bose stars comprised of a dilute BEC using the nonrelativistic GP equation (together with the Poisson equation) and perturbative solutions of such slowly rotating stars were obtained. Slowly rotating BEC stars in the Newtonian limit obeying a polytropic EOS have also been studied by solving the Lane-Emden equation [16]. The impact of slow rotation on the astrophysical properties of BEC dark matter halos were also determined using the nonrelativistic approach [39]. It was noted that the general relativistic effects impose strong constraints on the global parameters of the BEC stars and the obtained values within the nonrelativistic formalism may exceed this stability limit [14,40]. Relativistic BEC stars obeying the Colpi-Shapiro-Wasserman (CSW) EOS introduced in Ref. [41] were studied in Ref. [16] and it was speculated that the observed massive neutron stars [42,43] are composed of BECs. Further, the analysis of Ref. [16] was generalized to include spin and focused on studying the observational constraints on the structural properties of spinning relativistic BEC stars obeying the CSW EOS [44] by employing the rapidly rotating neutron star (RNS) code [45] based on general relativistic treatment. The electromagnetic and thermodynamic properties of thin accretion disks around rotating pure BEC stars with a polytropic EOS have been investigated in Ref. [40] by using the RNS code to obtain the rotating configurations of the star. In the present work, we intend to study the static and slowly rotating BEC stars by considering the general relativistic effects.

Further, BEC has been generalized to finite temperatures and has been studied in the contexts of cosmological dark matter [46,47] and static compact objects [48–50] recently. There are attempts to study boson stars with inclusion of chemical potential and temperatures [51–54]. The theory of condensate dynamics at finite temperature has been discussed in Refs. [55–57]. A finite temperature BEC has been considered in Ref. [47], which is composed of two fluids, the pure condensate and thermal fluctuations. An EOS at finite temperature describing such a BEC system has been obtained analytically. Further, they apply this description of the BEC to study the cosmological evolution of a finite temperature dark matter filled universe in a flat Friedmann-Robertson-Walker geometry. Pure BEC stars described by a thermodynamically consistent finite temperature EOS were considered and the global properties of a static BEC star were studied [48]. Recently, the astrophysical properties of relativistic BECs at finite temperature with the inclusion of

magnetic field were also investigated [50]. Further, Ref. [49] considers a BEC with repulsive contact and attractive gravitational interactions in the interior of neutron stars by the formation of Cooper pairs and macroscopic properties of the star have been evaluated at finite temperature. They describe the BEC stellar matter at the core to be composed of pure condensate together with a noncondensate cloud of excitations due to the presence of temperature. Analysis of pure BEC stellar equilibrium at finite temperature employing this EOS will be of interest. We note that, this finite temperature EOS is different from the one derived in Ref. [48] based on a thermodynamical method. Moreover, the study of macroscopic properties of rotating BEC stars at finite temperature has not been attempted before. This sets the motivation for the present analysis.

In the current work, we intend to analyze the effect of temperature on the global properties of static and rotating BEC stars. We employ the recently developed finite temperature BEC equation of state for the stellar matter obtained using the generalized GP equation with repulsive contact and attractive gravitational interactions with approximations based on the semiclassical Hartree-Fock theory [49]. The stellar matter now is considered to be composed of a Bose condensed state together with a small fraction of excitations of a BEC due to the presence of temperature. In our analysis, we treat gravity within the framework of general relativity. The properties of static BEC stars are analyzed for different temperatures by solving the Tolman-Oppenheimer-Volkoff equations [58,59]. We include rotation in the analysis through the Hartle-Thorne slow rotation approximation [60,61], which is a well-known perturbative approach and has been widely used in studies of compact objects [62–64]. To the best of our knowledge, this appropriate relativistic slow rotation approximation has not been employed so far to study BEC stars.

The paper is organized as follows. In Sec. II, we review the BEC equation of state at finite temperature used for the analysis. Then, we discuss the general relativistic stellar structure equations for static and slowly rotating stars in Sec. III. Next, we present the results in Sec. IV. Finally, we summarize our results and conclusions in the last section.

II. EQUATION OF STATE FOR A FINITE TEMPERATURE BEC

In this section, we briefly review the formalism to estimate the equation of state for a nonrotating BEC subjected to repulsive contact and attractive gravitational interactions at finite temperature as derived in Ref. [49]. The formalism to describe such a nonrotating BEC system is based on the studies in Refs. [55–57]. At zero temperature, a BEC is described by a macroscopic wave function $\Psi(\mathbf{r}, t)$, whose evolution is given by the GP equation [10,11]. A finite temperature BEC system consists of condensate particles together with a noncondensate cloud of thermal fluctuations [47,49,56]. The thermal cloud comprises

excitations from the condensate due to the presence of temperature and these excitations vanish with the decrease in temperature resulting in a system with pure condensate. The description of such a system begins by considering a BEC at zero temperature and extending it to finite temperature.

The dynamics of a Bose-Einstein condensate is described by the Heisenberg equation of motion for the Bose field operator $\hat{\psi}(\mathbf{r}, t)$ and is given by [11,55,56]

$$i\hbar \frac{\partial \hat{\psi}(\mathbf{r}, t)}{\partial t} = \left[-\frac{\hbar^2}{2m}\nabla^2 + \Phi(\mathbf{r}, t) \right.$$
$$\left. + g\hat{\psi}^\dagger(\mathbf{r}, t)\hat{\psi}(\mathbf{r}, t) \right]\hat{\psi}(\mathbf{r}, t), \qquad (1)$$

where $\Phi(\mathbf{r}, t)$ is the Newtonian gravitational potential. The quantity $g = 4\pi a\hbar^2/m$ represents the strength of the repulsive contact interaction with a being the s-wave scattering length of bosons in the system; m denotes the mass of condensate particles and G is Newton's gravitational constant. The Heisenberg equation is extended to finite temperature by considering the effects of noncondensate atoms, referred to as the thermal cloud, along with the condensate particles. Now, by assuming Bose broken symmetry, the field operator can be decomposed as [55]

$$\hat{\psi}(\mathbf{r}, t) = \Psi(\mathbf{r}, t) + \hat{\Psi}_{\text{th}}(\mathbf{r}, t), \qquad (2)$$

where, the expectation value of the Bose field operator denotes the condensate wave function $\Psi(\mathbf{r}, t) \equiv \langle \hat{\psi}(\mathbf{r}, t)\rangle$ and $\hat{\Psi}_{\text{th}}(\mathbf{r}, t)$ is the noncondensate field operator with $\langle \hat{\Psi}_{\text{th}}(\mathbf{r}, t)\rangle = 0$. By taking the average of Eq. (1) with respect to a broken symmetry nonequilibrium ensemble, we obtain an exact equation of motion for the condensate wave function $\Psi(\mathbf{r}, t)$ given by [55]

$$i\hbar \frac{\partial \Psi(\mathbf{r}, t)}{\partial t} = \left[-\frac{\hbar^2}{2m}\nabla^2 + \Phi(\mathbf{r}, t) \right]\Psi(\mathbf{r}, t)$$
$$+ g\left\langle \hat{\psi}^\dagger(\mathbf{r}, t)\hat{\psi}(\mathbf{r}, t)\hat{\psi}(\mathbf{r}, t)\right\rangle. \qquad (3)$$

Considering the expansion of the term,

$$\hat{\psi}^\dagger(\mathbf{r}, t)\hat{\psi}(\mathbf{r}, t)\hat{\psi}(\mathbf{r}, t) = |\Psi|^2\Psi + 2|\Psi|^2\hat{\Psi}_{\text{th}} + \Psi^2\hat{\Psi}^\dagger_{\text{th}}$$
$$+ 2\Psi\hat{\Psi}^\dagger_{\text{th}}\hat{\Psi}_{\text{th}} + \Psi^\dagger\hat{\Psi}_{\text{th}}\hat{\Psi}_{\text{th}}$$
$$+ \hat{\Psi}^\dagger_{\text{th}}\hat{\Psi}_{\text{th}}\hat{\Psi}_{\text{th}}, \qquad (4)$$

we proceed to find its expectation value by noting the number densities of the condensate and the thermal cloud respectively as

$$n(\mathbf{r}, t) = \langle \Psi^\dagger(\mathbf{r}, t)\Psi(\mathbf{r}, t)\rangle, \qquad (5)$$

$$n_{\text{th}}(\mathbf{r}, t) = \langle \hat{\Psi}^\dagger_{\text{th}}(\mathbf{r}, t)\hat{\Psi}_{\text{th}}(\mathbf{r}, t)\rangle. \qquad (6)$$

The second and third terms on the right-hand side of Eq. (4) vanish, since the average value of thermal fluctuations is zero because of the assumed broken symmetry. Further, by denoting the mass densities of condensate and noncondensate parts as $\rho(\mathbf{r}, t) = mn(\mathbf{r}, t)$ and $\rho_{\text{th}}(\mathbf{r}, t) = mn_{\text{th}}(\mathbf{r}, t)$ respectively, and the off-diagonal (anomalous) mass density as $\rho_a(\mathbf{r}, t) = mn_a(\mathbf{r}, t) = m\langle \hat{\Psi}_{\text{th}}(\mathbf{r}, t)\hat{\Psi}_{\text{th}}(\mathbf{r}, t)\rangle$, we get the following expression:

$$\left\langle \hat{\psi}^\dagger(\mathbf{r}, t)\hat{\psi}(\mathbf{r}, t)\hat{\psi}(\mathbf{r}, t)\right\rangle = \frac{1}{m}\rho\Psi + 2\frac{1}{m}\rho_{\text{th}}\Psi$$
$$+ \frac{1}{m}\rho_a\Psi^\dagger + \left\langle \hat{\Psi}^\dagger_{\text{th}}\hat{\Psi}_{\text{th}}\hat{\Psi}_{\text{th}}\right\rangle. \quad (7)$$

Substituting Eq. (7) in Eq. (3) yields the equation of motion for Ψ—the generalized GP equation [56]:

$$i\hbar \frac{\partial \Psi(\mathbf{r}, t)}{\partial t} = \left[-\frac{\hbar^2}{2m}\nabla^2 + \Phi(\mathbf{r}, t) + gn(\mathbf{r}, t) \right.$$
$$\left. + 2gn_{\text{th}}(\mathbf{r}, t) \right]\Psi(\mathbf{r}, t) + gn_a(\mathbf{r}, t)\Psi^\dagger(\mathbf{r}, t)$$
$$+ g\left\langle \hat{\Psi}^\dagger_{\text{th}}(\mathbf{r}, t)\hat{\Psi}_{\text{th}}(\mathbf{r}, t)\hat{\Psi}_{\text{th}}(\mathbf{r}, t)\right\rangle. \qquad (8)$$

We now assume a Madelung representation of the condensate wave function with the phase term $S(\mathbf{r}, t)$ having dimension of action [11],

$$\Psi(\mathbf{r}, t) = \sqrt{n(\mathbf{r}, t)}e^{(i/\hbar)S(\mathbf{r}, t)}. \qquad (9)$$

Here, the phase factor is related to the velocity of the condensate as $\mathbf{v}(\mathbf{r}, t) = \nabla S/m$. Substitution of the above form of the wave function in the generalized GP equation, Eq. (8), results in two equations corresponding to real and imaginary parts as [56]

$$\frac{\partial n}{\partial t} + \boldsymbol{\nabla}\cdot(n\mathbf{v}) = \frac{2g}{\hbar}\text{Im}\left[(\Psi^\dagger)^2 n_a + \Psi^\dagger\left\langle \hat{\Psi}^\dagger_{\text{th}}\hat{\Psi}_{\text{th}}\hat{\Psi}_{\text{th}}\right\rangle\right]$$

$$\frac{\partial S}{\partial t} = \frac{\hbar^2}{2m\sqrt{n}}\nabla^2\sqrt{n} - \Phi(\mathbf{r}, t) - gn(\mathbf{r}, t)$$
$$- 2gn_{\text{th}}(\mathbf{r}, t) - \frac{g}{n}\text{Re}\left[(\Psi^\dagger)^2 n_a \right.$$
$$\left. + \Psi^\dagger\left\langle \hat{\Psi}^\dagger_{\text{th}}\hat{\Psi}_{\text{th}}\hat{\Psi}_{\text{th}}\right\rangle\right] - \frac{1}{2}mv^2. \qquad (10)$$

Now, using the several approximation schemes, as discussed in Ref. [49] and references therein, we simplify the above obtained equations. We can utilize the Hartree-Fock-Bogoliubov approximation to ignore the three-field correlation function $\langle \hat{\Psi}^\dagger_{\text{th}}\hat{\Psi}_{\text{th}}\hat{\Psi}_{\text{th}}\rangle$. The dynamic Popov approximation can be used to ignore both $\langle \hat{\Psi}^\dagger_{\text{th}}\hat{\Psi}_{\text{th}}\hat{\Psi}_{\text{th}}\rangle$ and anomalous mass density $\rho_a(\mathbf{r}, t)$. With the static Popov approximation, the fluctuations of the density of the thermal cloud are ignored by assuming that the

noncondensate is always in static thermal equilibrium, so that $n_{\text{th}}(\mathbf{r}, t) \simeq n_{\text{th}}(\mathbf{r})$. Further, the time dependence in all other terms is neglected [49]. Now, using these approximations, Eq. (10) take the form of hydrodynamic continuity and Euler equations [56]

$$\frac{\partial n}{\partial t} + \boldsymbol{\nabla} \cdot (n\mathbf{v}) = 0, \tag{11}$$

$$mn\left[\frac{\partial \mathbf{v}}{\partial t} + \boldsymbol{\nabla}\left(\frac{v^2}{2}\right)\right] = \frac{\hbar^2}{2m\sqrt{n}} \nabla^2 \sqrt{n} - n\boldsymbol{\nabla}\Phi(\mathbf{r})$$
$$- gn\boldsymbol{\nabla}(n + 2n_{\text{th}}), \tag{12}$$

respectively. Further, we adopt the Thomas-Fermi approximation [46], which neglects the kinetic energy term of the condensate i.e., $-\hbar^2\nabla^2/2m$. Therefore, the quantum correction stress tensor term proportional to $\nabla^2\sqrt{n}$ in Eq. (12) also gets neglected. Equation (12) is compared with the general Euler equation to obtain the gradient of condensate pressure as [49]

$$\boldsymbol{\nabla}p = gn\boldsymbol{\nabla}(n + 2n_{\text{th}}). \tag{13}$$

The expression for noncondensate density can be obtained by integrating the Bose-Einstein distribution over the momentum space in spherical polar coordinates (r_k, θ_k, ϕ_k),

$$n_{\text{th}}(r_k) = \int \frac{d^3k}{(2\pi)^3} \frac{1}{e^{\beta[\epsilon_k(r_k)-\mu]} - 1}, \tag{14}$$

where, $\epsilon_k(r_k)$ represents the energy of the thermal excitations and μ denotes the chemical potential of the condensate. Here, $\beta = (k_BT)^{-1}$, with T as the temperature of the system and k_B as the Boltzmann constant. Now, to evaluate Eq. (14), we employ the semiclassical Hartree-Fock equations of motion for a system with contact and gravitational interactions [49],

$$\epsilon_k(r_k) = \frac{\hbar^2k^2}{2m} + 2g[n(r_k) + n_{\text{th}}(r_k)] + \Phi(r_k), \tag{15}$$

$$\mu = g[n(r_k) + 2n_{\text{th}}(r_k)] + \Phi(r_k), \tag{16}$$

where $\Phi(r_k)$ is now given by

$$\Phi(r_k) = -\int d^3r'_k \frac{Gm^2}{|r_k - r'_k|}[n(r'_k) + n_{th}(r'_k)]. \tag{17}$$

Using the above relations in the expression for thermal density and solving with the help of standard integrals, we get

$$n_{\text{th}}(r_k) = \frac{1}{\lambda^3}\zeta_{3/2}\left[e^{-\beta gn(r_k)}\right], \tag{18}$$

where $\lambda = \sqrt{(2\pi\beta\hbar^2)/m}$ is the thermal de Broglie wavelength and ζ represents the polylogarithmic function

$$\zeta_\nu[z] = \sum_{n=1}^{\infty} \frac{z^n}{n^\nu}, \tag{19}$$

with index ν. Substituting Eq. (18), we integrate out Eq. (13) to obtain the pressure of the condensate including the effects of the thermal cloud [49]:

$$p = \frac{g\rho^2}{2m^2} + \frac{2g\rho}{m\lambda^3}\zeta_{3/2}[e^{-\beta g\rho/m}]$$
$$+ \frac{2}{\beta\lambda^3}\zeta_{5/2}[e^{-\beta g\rho/m}] - \frac{2}{\beta\lambda^3}\zeta_{5/2}[1]. \tag{20}$$

Here, the first term denotes the pressure of the pure condensate in the absence of thermal fluctuations. The second and third terms represent the contribution of thermal excitations to the pressure of the condensate. Further, the constant term ensures that the condensate pressure vanishes in the limit $\rho \to 0$.

We plot the above obtained BEC EOS for different temperatures in Fig. 1. Here, we take the mass of the condensate particle to be $m = 2m_n$, where m_n is the mass of a nucleon, considering the possibility of two of them forming an equivalent Cooper pair and act as a boson [16]. The scattering length is taken to be $a = 1$ fm [49]. Also, following Ref. [49], in our studies, we focus on relevant temperatures of $(1-4) \times 10^{11}$ K.

In Fig. 1, the curve plotted for $T = 0$ K represents the pressure of pure condensate. Note that this corresponds to the polytropic EOS used in Ref. [16]. We observe that the presence of temperature in the system decreases the condensate pressure. This is due to the fact that temperature
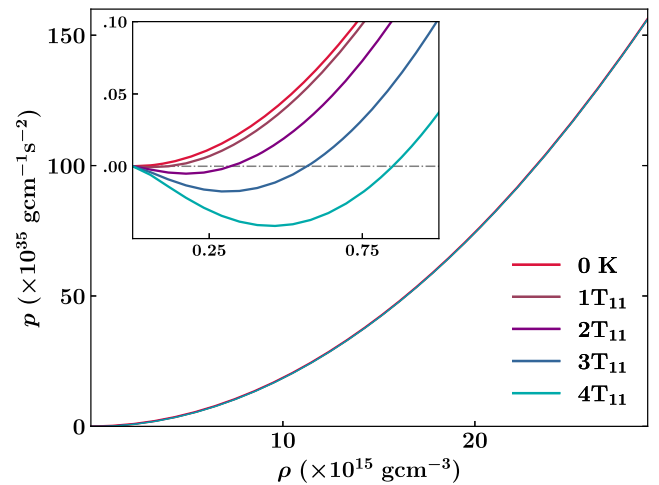

FIG. 1. BEC equation of state with the effect of thermal fluctuations for different temperatures. Inset highlights the effect of temperature in lower densities.

in the system results in thermal excitations of a few fractions of condensate particles. It can also be seen that the pressure becomes negative for small densities. This is a consequence of the Thomas-Fermi approximation, which neglected the quantum pressure term of the condensate in the calculations. This term becomes important at the edge of the star, where the density of the condensate is low. The addition of this quantum pressure term would presumably correct the unphysical negative pressure observed for small densities [49]. Moreover, we note that a zero-temperature treatment would be sufficient for temperatures below 10^{11} K, since the thermal fluctuations are negligible within that temperature range. Furthermore, Fig. 1 shows that although the presence of temperature decreases the pressure of the condensate for a fixed density, this decrement is observed to be very small implying a small deviation of the pressure from the $T = 0$ K case for the range of ρ values considered. For example, at $\rho = 2 \times 10^{16}$ g/cm^3, the deviation of the condensate pressure from the zero-temperature case is ~0.27% when $T = 4 \times 10^{11}$ K, while the deviation is only ~0.008% for $T = 1 \times 10^{11}$ K. The zero-temperature polytropic EOS has been employed to study rotating BEC stars within Newtonian [22] and general relativistic [40] treatments. In the present work, we introduce the effect of slow rotation to the finite temperature BEC system described by Eq. (20) via general relativistic treatment.

We now proceed to calculate the stellar configuration dynamic equations within the general theory of relativity to utilize the above-obtained temperature-dependent EOS to study BEC star profiles.

III. STELLAR STRUCTURE EQUATIONS

We employ a general relativistic treatment to study the stellar structure equations. We first calculate the nonrotating configurations of the star and then use them to obtain the slowly rotating configurations. In this section, we follow the metric convention $g_{\mu\nu} = \text{diag}(-1, 1, 1, 1)$ and use velocity of light $c = 1$. The metric for a spherically symmetric static relativistic star can be expressed as

$$ds^2 = -e^\nu dt^2 + e^\Lambda dr^2 + r^2(d\theta^2 + \sin^2\theta d\phi^2). \quad (21)$$

Here, $\nu(r)$ and $\Lambda(r)$ are the metric functions. Assuming the stellar matter to be described by perfect fluid with energy density ρ and pressure p, the Einstein field equations result in the Tolman-Oppenheimer-Volkoff (TOV) equations, which are given as [58,59]

$$\frac{dp}{dr} = -\frac{G(\rho + p)(M + 4\pi r^3 p)}{r^2(1 - 2GM/r)}, \quad (22a)$$

$$\frac{dM}{dr} = 4\pi r^2 \rho. \quad (22b)$$

The above coupled differential equations are solved from the center to the surface of the star by providing an equation of state for the stellar matter. We employ the EOS given by Eq. (20) with the assumption that the condensate can be described by a nonrelativistic EOS. The pressure and mass at the center of the star are $p_c = p(\rho_c)$ and $M_c = 0$ respectively. The pressure p vanishes as it approaches the surface ($r = R$) of the star. The mass of the star is then obtained as $M(r = R)$. By varying the central density ρ_c, we can get the maximum mass (radius) stellar configuration possible for the given EOS.

The solutions $p(r)$ and $M(r)$ obtained for a given central density are then used to solve for a slowly rotating BEC star. For this we make use of the Hartle-Thorne approximation [60,61] in which rotation is treated as a small perturbation on the metric of the nonrotating star:

$$\begin{aligned}
ds^2 = &-e^\nu[1 + 2(h_0 + h_2 P_2)]dt^2 \\
&+ \frac{1 + 2G(m_0 + m_2 P_2)(r - 2GM)^{-1}}{1 - 2GM/r}dr^2 \\
&+ r^2[1 + 2(v_2 - h_2)P_2][d\theta^2 + \sin^2\theta(d\phi - \omega dt)^2] \\
&+ O(\Omega^3).
\end{aligned} \quad (23)$$

Here, $P_2 = P_2(\cos\theta)$ is the second order Legendre polynomial, ω is the frame dragging frequency which is proportional to Ω and is a function of r, while h_0, m_0, h_2, m_2, p_2, and v_2 are functions of r that are proportional to Ω^2. The angular velocity relative to the local inertial frame $\bar{\omega}\ (= \Omega - \omega)$ is obtained by solving the second order differential equation

$$\frac{1}{r^4}\frac{d}{dr}\left(r^4 j \frac{d\bar{\omega}}{dr}\right) + \frac{4}{r}\frac{dj}{dr}\bar{\omega} = 0, \quad (24)$$

where

$$j = e^{-\nu/2}(1 - 2GM/r)^{1/2}. \quad (25)$$

Equation (24) is integrated from the center to the surface of the star with the boundary conditions: $\bar{\omega} = \omega_c$ and $d\bar{\omega}/dr = 0$. The angular momentum J and the angular velocity Ω corresponding to ω_c are

$$J = \frac{1}{6}R^4\left(\frac{d\bar{\omega}}{dr}\right)_{r=R}, \qquad \Omega = \bar{\omega}(R) + \frac{2J}{R^3}. \quad (26)$$

In order to obtain a different value of angular velocity, the function $\bar{\omega}(r)$ is rescaled as

$$\bar{\omega}(r)_{\text{new}} = \bar{\omega}(r)_{\text{old}}\left(\frac{\Omega_{\text{new}}}{\Omega_{\text{old}}}\right). \quad (27)$$

The deformation of stellar structure as a result of rotation can be obtained in terms of $\xi(r, \theta)$ [60,61]:

$$\xi(r,\theta) = \xi_0(r) + \xi_2(r)P_2. \tag{28}$$

Here, the first term corresponds to the spherical ($l = 0$) deformation and the second term corresponds to the quadrupole ($l = 2$) deformation. In our study, we focus only on the spherical deformation $\xi_0(r)$, which can be obtained by solving the mass perturbation factor (m_0) and the pressure perturbation factor (p_0^*) equations given as [60,61]

$$\frac{dm_0}{dr} = 4\pi r^2 \frac{d\rho}{dp}(\rho + p)p_0^* + \frac{1}{12G}j^2 r^4 \left(\frac{d\bar{\omega}}{dr}\right)^2$$
$$- \frac{1}{3G}r^3 \frac{dj^2}{dr}\bar{\omega}^2, \tag{29a}$$

$$\frac{dp_0^*}{dr} = -\frac{Gm_0(1 + 8\pi Gr^2 p)}{r^2(1 - 2GM/r)^2} - \frac{4\pi G(\rho + p)r}{(1 - 2GM/r)}p_0^*$$
$$+ \frac{1}{12}\frac{r^3 j^2}{(1 - 2GM/r)}\left(\frac{d\bar{\omega}}{dr}\right)^2 + \frac{1}{3}\frac{d}{dr}\left(\frac{r^2 j^2 \bar{\omega}^2}{1 - 2GM/r}\right). \tag{29b}$$

The above differential equations are to be integrated from the center to the surface of the star, with the boundary conditions that at the center of the star $m_0 = p_0^* = 0$. The density profile of the slowly rotating star is then obtained as

$$\rho_{\rm rot}(r) = \rho_{\rm stat}(r) - \frac{d\rho_{\rm stat}(r)}{dr}\xi_0(r), \tag{30}$$

where

$$\xi_0(r) = -p_0^*(r)\frac{\rho(r) + p(r)}{dp(r)/dr}. \tag{31}$$

The gravitational mass (M^*) and the radius (R^*) of the slowly rotating star are given by

$$M^* = M(R) + m_0(R) + \frac{J^2}{R^3}, \tag{32a}$$

$$R^* = R + \xi_0(r). \tag{32b}$$

Here, $M(R)$ and R are the mass and radius of a static star obtained from TOV equations for a given central density.

Once we prescribe the equation of state by solving the above obtained set of equations for static and rotating cases, the corresponding stellar structure configurations can be obtained.

IV. RESULTS AND DISCUSSION

We numerically integrate the coupled stellar structure differential equations given by Eqs. (22a), (22b) and Eqs. (29a), (29b) using the temperature-dependent BEC EOS, Eq. (20), to obtain the static and rotating stellar
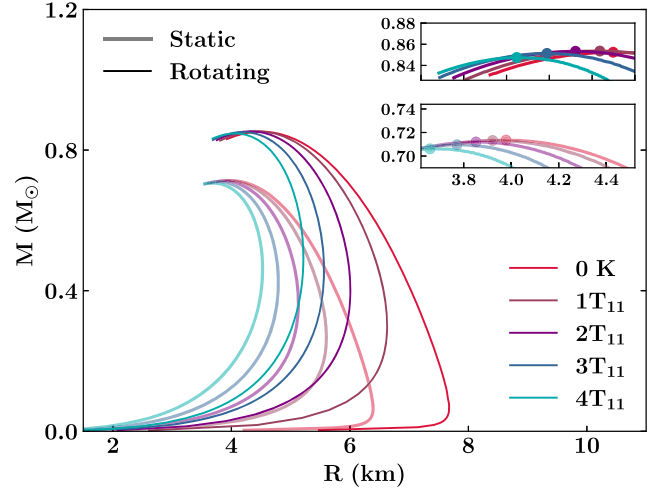

FIG. 2. Mass of the BEC star as a function of the radius for different temperatures ($T_{11} = 10^{11}$ K). The dashed curves correspond to the static stellar configurations. Solid curves correspond to the BEC star configurations rotating slowly with their Keplerian angular velocity Ω_K. Inset shows the maximum masses in each case.

configurations respectively. For brevity, we have used M and R to denote the maximum mass and corresponding radius in both static and rotating cases. We are ignoring the possibility of formation of vortices in this analysis [39,40]. We study the global properties of these configurations for different temperature values as taken in Sec. II, ranging from $1T_{11}$ to $4T_{11}$, where $T_{11} = 10^{11}$ K. As noted before [49], a zero-temperature treatment would be sufficient for temperatures below 10^{11} K as the effect of temperature on the EOS is negligible in that range. Initially we keep $m = 2m_n$, where $m_n = 1.675 \times 10^{-24}$ g is the mass of a nucleon and scattering length as $a = 1$ fm in our analysis.

In Fig. 2, we plot the mass of both the static and slowly rotating BEC stars as a function of the radius corresponding to different temperatures. For the static case, at $T = 0$ K, we obtain a maximum mass $M = 0.71M_\odot$, with $M_\odot$ being the mass of the Sun, with radius $R = 3.97$ km corresponding to the central density $\rho_c = 2.03 \times 10^{16}$ g/cm³. Our results are in agreement with the zero-temperature static general relativistic BEC stars studied in Ref. [16]. While coming to the finite temperature case, we see that static stellar equilibria are achieved at reduced radii and masses, though the form of the mass-radius curve does not change appreciably. For example, the radii corresponding to a $0.65M_\odot$ star are 4.71, 4.56, 4.40, and 4.24 km respectively for the temperatures $T = (1, 2, 3, 4)T_{11}$. This is due to the fact that an increase in temperature results in a lower value of pressure for a given energy density (see inset of Fig. 1), implying a softer equation of state. Softening of the EOS is a consequence of the presence of thermal fluctuations in the star. A softer EOS is known to result in lower maximum mass-radius models [33]. Interestingly, the maximum mass
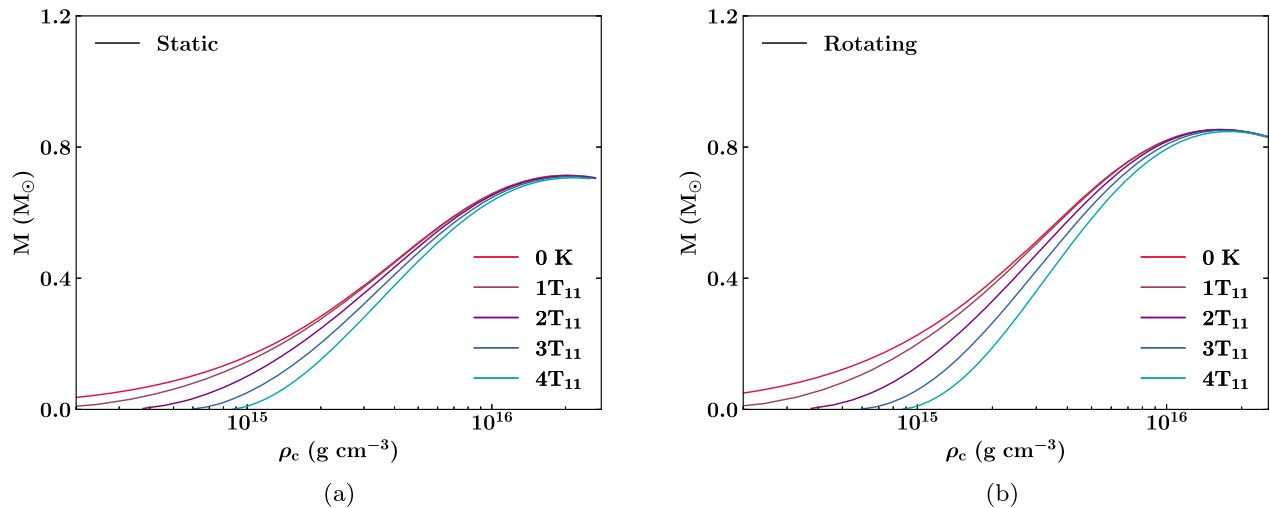
FIG. 3. Mass of the (a) static and (b) slowly rotating stellar configurations as a function of the central density for different temperatures $(T_{11} = 10^{11}$ K$)$.

and corresponding radius of the static BEC star does not vary significantly for the different temperatures considered in our analysis from the zero-temperature case, as seen from the inset of the figure. The maximum mass values corresponding to the temperatures $(1, 2, 3, 4)T_{11}$ are 0.71, 0.71, 0.71, and $0.70M_\odot$ respectively. We note that this particular behavior was observed in the study conducted on static BEC stars at finite temperature employing a different EOS in Ref. [48].

Further, in Fig. 2, we have expanded our analysis to incorporate rotation into the system. We allow the stellar equilibria to rotate in their Keplerian angular velocity $\Omega_K = \sqrt{GM/R^3}$, where M and R denote the maximum mass and maximum radius of the static configurations. Incorporating rotation into a system is likely to result in an additional centrifugal force. As a consequence of this, in order to maintain gravitational equilibrium, an increase in the maximum mass is anticipated and it is numerically obtained as $M = 0.85M_\odot$ for the zero-temperature case. This value corresponds to the central density $\rho_c = 1.6 \times 10^{16}$ g/cm^3 and radius $R = 4.47$ km. Mere rotation increases the mass-radius profiles and maximum mass and radius of the star compared to the static case. However, as seen in the static case, increasing the system temperature results in a reduction of mass-radius curves (due to softening of the EOS) in rotational case too. The radii corresponding to a $0.8M_\odot$ star are 5.28, 5.08, 4.87, and 4.66 km respectively for the temperatures $T = (1, 2, 3, 4)T_{11}$. In the rotating case too, we report that the maximum mass and radius for the stellar equilibria are not much altered by the presence of the temperature considered. As seen from the inset of Fig. 2, the maximum masses corresponding to the temperature considered $(1, 2, 3, 4)T_{11}$ are 0.85, 0.84, 0.84, and $0.84M_\odot$ respectively. We note that Ω_K corresponding to the BEC stars with temperature $T = (0, 1, 2, 3, 4)T_{11}$ is

$(3.89, 3.96, 4.07, 4.19, 4.37) \times 10^4$ s^{-1} respectively for their maximum mass configurations.

Next, we plot the variation of mass with central density for the static and rotating BEC stars in Figs. 3(a) and 3(b) respectively. For both the static and rotating cases, the mass values obtained for the temperatures do not vary significantly at higher densities, whereas in the lower density region a significant difference is seen. The masses of rotating stars corresponding to $T = 0$ K and $T = 4 \times 10^{11}$ K are obtained as $M = 0.39M_\odot$ and $M = 0.18M_\odot$ respectively, for $\rho_c = 2 \times 10^{15}$ g/cm^3. While for the static case, the masses corresponding to $T = 0$ K and $T = 4 \times 10^{11}$ K are obtained as $M = 0.28M_\odot$ and $M = 0.15M_\odot$ respectively, with the same value of central density. The maximum mass value configurations for $T = 0$ K in the static and rotating cases correspond to central densities 2.03×10^{16} and 1.6×10^{16} g/cm^3 respectively. Introduction of temperature results in an increase in the central density value corresponding to maximum masses. In the static case, the central density values corresponding to the maximum mass for the temperatures $(1, 2, 3, 4) \times 10^{11}$ K are $(2.05, 2.06, 2.09, 2.20) \times 10^{16}$ g/cm^3 respectively. And for the rotating case the maximum mass for the temperatures $(1, 2, 3, 4) \times 10^{11}$ K corresponds to the central densities $(1.61, 1.65, 1.71, 1.79) \times 10^{16}$ g/cm^3 respectively. We also note that, with the increment in central densities, mass of the configurations also increases, while the corresponding radii decrease.

As we study the relationship between angular velocity and mass in rotating systems, we notice that the difference between static star and rotational mass grows with increasing angular velocity as illustrated in Fig. 4. This can be attributed to the fact that the increase in mass caused by rotation is directly proportional to the angular velocity. As the angular velocity increases, it results in a corresponding
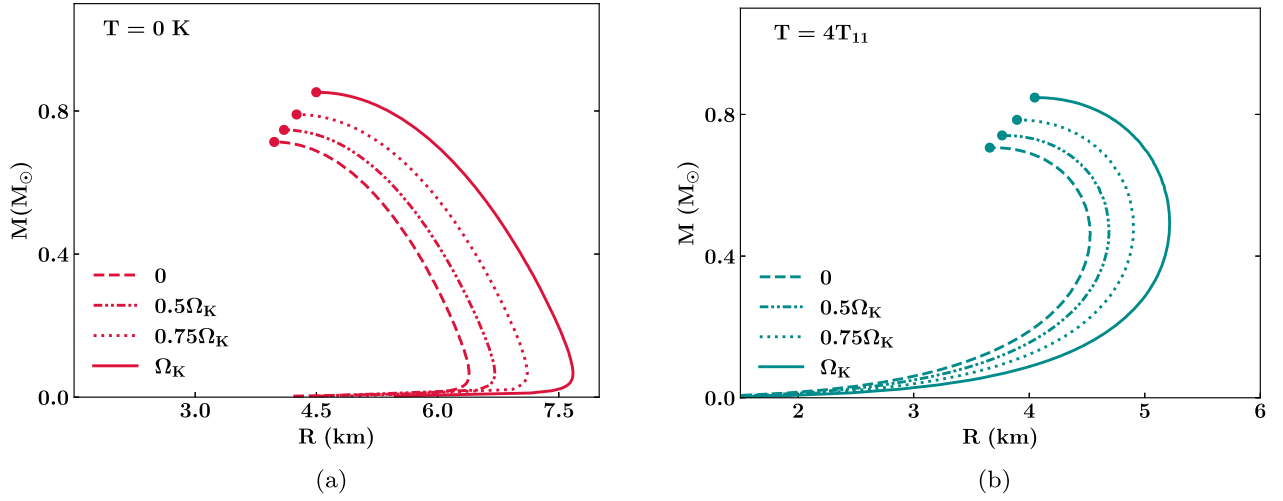
FIG. 4. Mass of the slowly rotating BEC star as a function of the radius by varying the angular velocities, for (a) $T = 0$ K and (b) $T = 4T_{11} = 4 \times 10^{11}$ K.

increase in the centrifugal force experienced within the system. To counterbalance this augmented centrifugal force, a larger mass is required. We can read out from Fig. 4 that as we increase the angular velocity from zero to $0.5\Omega_K$ and $0.75\Omega_K$, the maximum mass correspondingly increases to $M = 0.75M_\odot$ and $M = 0.79M_\odot$ respectively. The radius values obtained for the same are $R = 4.09$ km and $R = 4.25$ km respectively. A similar trend is observed for finite temperatures. As the star starts rotating and when the angular velocities increase from $\Omega = 0.5\Omega_K$ to $\Omega = 0.75\Omega_K$, the maximum mass and corresponding radius values increase from $M = 0.74M_\odot$ to $M = 0.78M_\odot$ and $R = 3.76$ km to $R = 3.89$ km respectively, for $T = 4T_{11}$. We also note that due to the presence of temperature the star attains a larger mass at lower densities compared to the zero-temperature case for all values of angular velocities considered. It must be highlighted that the relativistic treatment is quite important while considering the global properties of BEC stellar models. The mass of the static BEC star obtained by solving the Newtonian Lane-Emden equation for $\rho_c = 4 \times 10^{15}$ g/cm^3 is $0.74M_\odot$ and the corresponding slow rotation (with $\Omega_K = 1.84 \times 10^4$ s^{-1}) gives the value $1.11M_\odot$ [65], whereas, within our general relativistic treatment, correspondingly, we get the mass values as 0.45 and $0.60M_\odot$ for static and slow rotation, respectively.

Further, we study the effect of condensate mass m on the static and rotating stellar configurations at finite temperature. First, we plot the BEC EOS for different values of boson mass: $m = 2m_n$ and $m = 1.5m_n$, with zero and finite temperatures in Fig. 5. We can see that, the lower the value of m, pressure increases for a given value of density resulting in a stiffer EOS. With $T = 4T_{11}$ and for $m = 1.5m_n$, the EOS remains stiffer even compared to the zero-temperature $m = 2m_n$ case. However, as observed

in Fig. 1, the presence of temperature has a relative softening effect.

In Fig. 6, we present the mass-radius relation by varying the value of m, for the $T = 0$ and $T = 4T_{11}$ cases. Evidently the mass and radius of the star depend quite sensitively on the condensate mass m considered. At zero temperature, on decreasing the mass of the condensate from $m = 1.5m_n$ to $m = 1.25m_n$, the maximum mass and corresponding radius increased from 1.10 to $1.44M_\odot$ and 6.12 to 8.04 km, for the static system and 1.31 to $1.72M_\odot$ and 6.93 to 9.06 km, for the rotating case, respectively. Also plotted for reference are the previously considered $m = 2m_n$ cases. A similar trend is observed for the finite temperature case. For the $T = 4T_{11}$ case, the maximum mass and radius increased from 1.08 to $1.42M_\odot$ and 5.58 to 7.24 km, for the static case, and 1.29 to $1.70M_\odot$ and 6.10 to 7.89 km, for the rotating case. The central
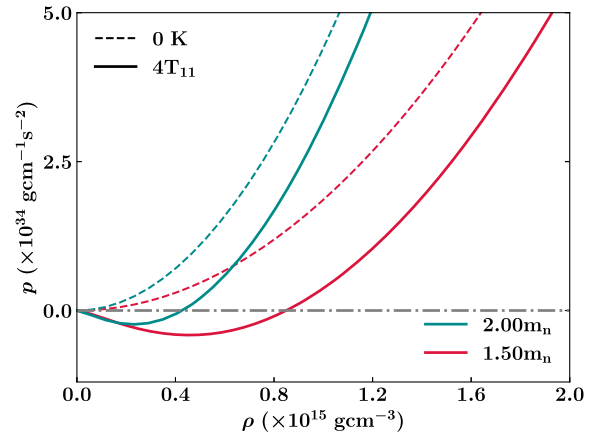

FIG. 5. BEC equation of state with different values of mass m for $T = 0$ K and $T = 4 \times 10^{11}$ K.
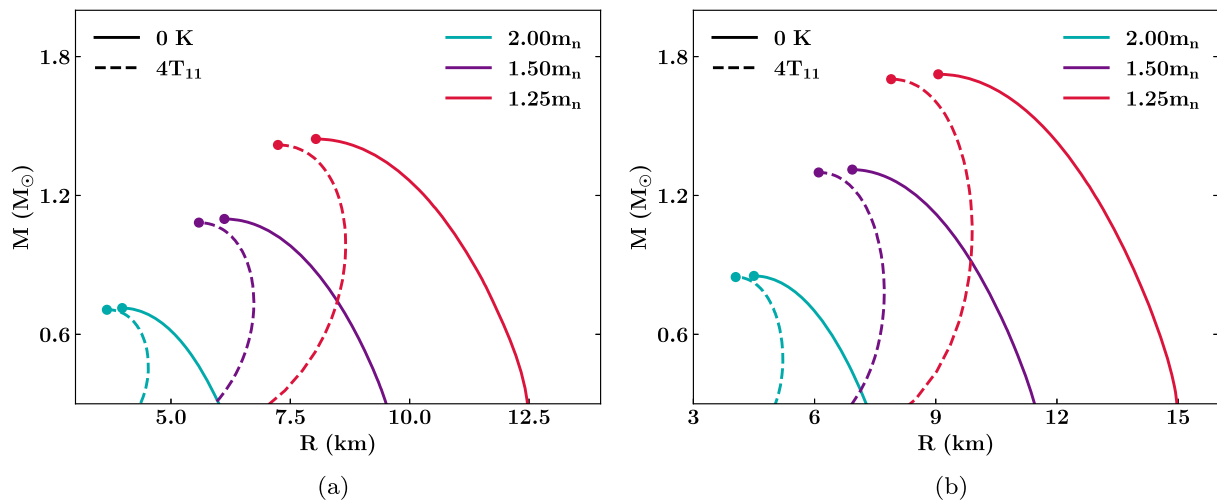
FIG. 6. Mass-radius relations of (a) static and (b) rotating BEC stars for different values of the condensate mass m (in terms of the nucleon mass m_n) at zero and finite temperature. Scattering length is kept as $a = 1$ fm.

density at which the maximum mass achieved for $m = 1.5m_n$ is $\rho_c = 8.55 \times 10^{15}$ g/cm^3 and $\rho_c = 6.79 \times 10^{15}$ g/cm^3 for the static and rotating systems respectively at zero temperature. At $T = 4T_{11}$, the central density at which the maximum mass obtained is $\rho_c = 9.17 \times 10^{15}$ g/cm^3 and $\rho_c = 7.78 \times 10^{15}$ g/cm^3 for the static and rotating systems respectively. The central density at which the maximum mass achieved for $m = 1.25m_n$ is $\rho_c = 4.95 \times 10^{15}(5.43 \times 10^{15})$ g/cm^3 and $\rho_c = 4 \times 10^{15}(4.60 \times 10^{15})$ g/cm^3 for the static and rotating systems respectively at $T = 0(4T_{11})$. The zero-temperature results obtained above are in agreement with that of Ref. [16]. As observed earlier, when the m value decreases, the EOS becomes more and more stiffer, and a stiffer EOS is known to exhibit higher mass and radius. When temperature is included a relative softening of the EOS happens resulting in a corresponding small decrease in the maximum mass. We also observe that, as the value of m gets decreased, although the difference between maximum masses obtained at each temperatures does not vary significantly for both the static and rotating cases, the difference between the corresponding radii keeps on increasing.

Finally, we proceed to study the effect of interaction between the bosons on the stellar profiles. We change the coupling constant of interaction $g \propto a/m$ in the EOS and solve the stellar structure equations for both static and rotating cases at finite temperature. By varying the value of the interaction strength from $g = 4.17 \times 10^{-43}$ g cm^5/s^2 to $0.5g$, $0.1g$, and $0.01g$, the maximum mass is observed to be decreasing from $0.71M_\odot$ to 0.50, 0.23, and $0.07M_\odot$ ($0.85M_\odot$ to 0.60, 0.27, and $0.08M_\odot$) respectively for the static (rotating) case at $T = 4T_{11}$. This gradual decrease in maximum mass is depicted in Fig. 7. We note that the mass-radius curves are highly sensitive to the interaction strength

and reduction of the same results in smaller maximum masses. As shown before, the inclusion of rotation increases the mass of the system relatively for any given value of g. The self-interaction arising due to the repulsive interaction between the individual particles within the condensate creates an effective outward pressure that counterbalances the gravitational collapse. If the self-interaction strength decreases, the effective pressure diminishes, and the force of gravity becomes dominant. As a result, the maximum mass that the BEC star can sustain decreases, as expected. This inference can be drawn from Eq. (20), when self-interaction is turned off the total outward pressure of the system against gravity vanishes, leading to an unstable configuration. This expected observation is in agreement with Ref. [49]. Moreover, as we decrease the strength of self-interaction, the difference
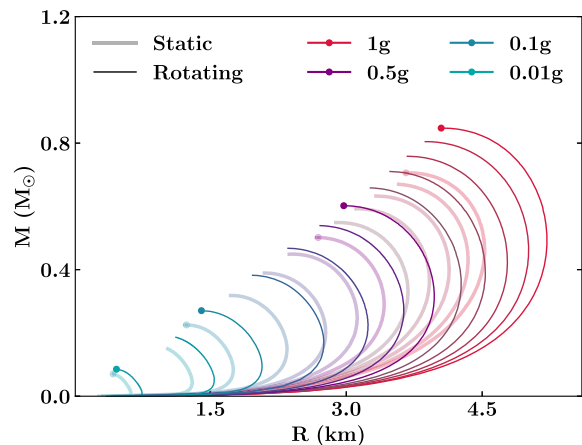

FIG. 7. Mass of the static and rotating BEC stars as a function of the radius for $T = 4 \times 10^{11}$ K by varying the interaction strength g.

between maximum masses attained for the static and rotating cases diminishes for any temperature.

V. SUMMARY AND CONCLUSIONS

We have investigated the global properties of static and slowly rotating Bose-Einstein condensate stars at finite temperature. To incorporate the effect of temperature into the analysis, we have used the recently developed finite temperature BEC EOS for the stellar matter derived from the generalized Gross-Pitaevskii equation for the condensate and thermal fluctuations. Gravity is treated in the framework of general relativity by using the Hartle-Thorne approximation for rotation.

Our numerical analysis shows that, although the impact of temperature considered is minimal on the EOS of a BEC star, it is observed that the mass and radius of static and rotating BEC stellar configurations are highly sensitive to the temperature of the system. The effect of an increment of temperature is to reduce the mass and radius of the system; however at lower central densities finite temperature supports higher values of mass. Further, the introduction of rotation results in higher mass-radius stellar systems. Our analysis has indicated that ignoring the general relativistic treatment of rotation results in an erroneous estimation of global properties of BEC stars.

Interestingly, we have found that the presence of thermal fluctuations has negligible impact on maximum masses of the static as well as rotating BEC stars, although considerable change in maximum radii are seen. We have also studied the effect of different rotational frequencies on the system. Further, together with the interplay of temperature and rotation, we have analyzed the effect of various EOS parameters, namely condensate mass and self-interaction strength, on the BEC star and quantified the results.

The agreement between our results and that of a non-rotating general relativistic BEC star at finite temperature considered in Ref. [48] suggests that the maximum mass of the star remains unaffected by changes in temperature even in the rotating case. On the other hand, their utilization of a different EOS leads them to anticipate a distinct trend in the mass-radius behavior. Considering the difference in their theoretical approach, leading to a stiffer EOS with the increasing temperatures, a close comparison with our present work is irrelevant. Furthermore, inclusion of the effect of magnetic field in the static finite temperature BEC star also reports minimal effect on the maximum mass [50]. In the future, we would like to extend our studies by incorporating magnetic field into the finite temperature BEC star system. Also, the possibility of rotating neutron stars with different exotic matter with such a BEC at its core will be of interest.

ACKNOWLEDGMENTS

[1] Georges Aad *et al.*, Observation of a new particle in the search for the standard model Higgs boson with the ATLAS detector at the LHC, Phys. Lett. B **716**, 1 (2012).

[2] Serguei Chatrchyan *et al.* (CMS Collaboration), Observation of a new boson at a mass of 125 GeV with the CMS experiment at the LHC, Phys. Lett. B **716**, 30 (2012).

[3] Philippe Jetzer, Boson stars, Phys. Rep. **220**, 163 (1992).

[4] Andrew R. Liddle and Mark S. Madsen, The structure and formation of boson stars, Int. J. Mod. Phys. D **01**, 101 (1992).

[5] Franz E. Schunck and Eckehard W. Mielke, General relativistic boson stars, Classical Quantum Gravity **20**, R301 (2003).

[6] Steven L. Liebling and Carlos Palenzuela, Dynamical boson stars, Living Rev. Relativity **26**, 1 (2023).

[7] James R. Anglin and Wolfgang Ketterle, Bose-Einstein condensation of atomic gases, Nature (London) **416**, 211 (2002).

[8] Iulia Georgescu, 25 years of BEC, Nat. Rev. Phys. **2**, 396 (2020).

[9] Franco Dalfovo, Stefano Giorgini, Lev P. Pitaevskii, and Sandro Stringari, Theory of Bose-Einstein condensation in trapped gases, Rev. Mod. Phys. **71**, 463 (1999).

[10] L. Pitaevskii and S. Stringari, *Bose-Einstein Condensation* (Clarendon Press, Oxford, 2003).

[11] C. Pethick and H. Smith, *Bose-Einstein Condensation in Dilute Gases* (Cambridge University Press, Cambridge, England, 2002).

[12] D. O'Dell, S. Giovanazzi, G. Kurizki, and V. M. Akulin, Bose-Einstein condensates with $1/r$ interatomic attraction: Electromagnetically induced "gravity", Phys. Rev. Lett. **84**, 5687 (2000).

[13] Kingsley R. W. Jones and David Bernstein, The self-gravitating Bose-Einstein condensate, Classical Quantum Gravity **18**, 1513 (2001).

[14] Pierre-Henri Chavanis, Mass-radius relation of Newtonian self-gravitating Bose-Einstein condensates with short-range interactions. I. Analytical results, Phys. Rev. D **84**, 043531 (2011).

[15] Pierre-Henri Chavanis and Luca Delfini, Mass-radius relation of Newtonian self-gravitating Bose-Einstein condensates with short-range interactions. II. Numerical results, Phys. Rev. D **84,** 043532 (2011).

[16] Pierre-Henri Chavanis and Tiberiu Harko, Bose-Einstein condensate general relativistic stars, Phys. Rev. D **86,** 064011 (2012).

[17] Pierre-Henri Chavanis, Partially relativistic self-gravitating Bose-Einstein condensates with a stiff equation of state, Eur. Phys. J. Plus **130,** 181 (2015).

[18] Felix Kling and Arvind Rajaraman, Towards an analytic construction of the wavefunction of boson stars, Phys. Rev. D **96,** 044039 (2017).

[19] Felix Kling and Arvind Rajaraman, Profiles of boson stars with self-interactions, Phys. Rev. D **97,** 063012 (2018).

[20] Lorenzo Annulli, Vitor Cardoso, and Rodrigo Vicente, Stirred and shaken: Dynamical behavior of boson stars and dark matter cores, Phys. Lett. B **811,** 135944 (2020).

[21] Pierre-Henri Chavanis, Maximum mass of relativistic self-gravitating Bose-Einstein condensates with repulsive or attractive $|\varphi|^4$ self-interaction, Phys. Rev. D **107,** 103503 (2023).

[22] C. G. Boehmer and T. Harko, Can dark matter be a Bose-Einstein condensate?, J. Cosmol. Astropart. Phys. 06 (2007) 025.

[23] Jae-Weon Lee and Sooil Lim, Minimum mass of galaxies from BEC or scalar field dark matter, J. Cosmol. Astropart. Phys. 01 (2010) 007.

[24] T. Harko, Bose-Einstein condensation of dark matter solves the core/cusp problem, J. Cosmol. Astropart. Phys. 05 (2011) 022.

[25] T. Harko, Evolution of cosmological perturbations in Bose-Einstein condensate dark matter, Mon. Not. R. Astron. Soc. **413,** 3095 (2011).

[26] Pierre-Henri Chavanis, Growth of perturbations in an expanding universe with Bose-Einstein condensate dark matter, Astron. Astrophys. **537,** A127 (2012).

[27] X. Y. Li, T. Harko, and K. S. Cheng, Condensate dark matter stars, J. Cosmol. Astropart. Phys. 06 (2012) 001.

[28] R. C. Freitas and S. V. B. Goncalves, Cosmological perturbations during the Bose-Einstein condensation of dark matter, J. Cosmol. Astropart. Phys. 04 (2013) 049.

[29] Tanja Rindler-Daller and Paul R. Shapiro, Complex scalar field dark matter on galactic scales, Mod. Phys. Lett. A **29,** 1430002 (2014).

[30] F. S. Guzmán, F. D. Lora-Clavijo, J. J. González-Avilés, and F. J. Rivera-Paleo, Rotation curves of rotating Galactic Bose-Einstein condensate dark matter halos, Phys. Rev. D **89,** 063507 (2014).

[31] Eniko J. M. Madarassy and Viktor T. Toth, Evolution and dynamical properties of Bose-Einstein condensate dark matter stars, Phys. Rev. D **91,** 044041 (2015).

[32] Joshua Eby, Chris Kouvaris, Niklas Grønlund Nielsen, and L. C. R. Wijewardhana, Boson stars from self-interacting dark matter, J. High Energy Phys. 02 (2016) 028.

[33] N. K. Glendenning, *Compact Stars: Nuclear Physics, Particle Physics, and General Relativity* (Springer, New York, 2000).

[34] C. J. Pethick, Thomas Schaefer, and A. Schwenk, Bose-Einstein condensates in neutron stars, arXiv:1507.05839.

[35] E. P. Gross, Structure of a quantized vortex in boson systems, Il Nuovo Cimento **20,** 454 (1961).

[36] Lev P Pitaevskii, Vortex lines in an imperfect Bose gas, Sov. Phys. JETP **13,** 451 (1961).

[37] Vanda Silveira and Claudio M. G. de Sousa, Boson star rotation: A Newtonian approximation, Phys. Rev. D **52,** 5724 (1995).

[38] Xian Zhi Wang, Cold bose stars: Self-gravitating Bose-Einstein condensates, Phys. Rev. D **64,** 124009 (2001).

[39] Xiaoyue Zhang, Man Ho Chan, Tiberiu Harko, Shi-Dong Liang, and Chun Sing Leung, Slowly rotating Bose Einstein condensate galactic dark matter halos, and their rotation curves, Eur. Phys. J. C **78,** 346 (2018).

[40] Bogdan Dănilă, Tiberiu Harko, and Zoltán Kovács, Thin accretion disks around cold Bose-Einstein condensate stars, Eur. Phys. J. C **75,** 203 (2015).

[41] M. Colpi, S. L. Shapiro, and I. Wasserman, Boson stars: Gravitational equilibria of self-interacting scalar fields, Phys. Rev. Lett. **57,** 2485 (1986).

[42] Paul Demorest, Tim Pennucci, Scott Ransom, Mallory Roberts, and Jason Hessels, A two-solar-mass neutron star measured using Shapiro delay, Nature (London) **467,** 1081 (2010).

[43] John Antoniadis *et al.*, A massive pulsar in a compact relativistic binary, Science **340,** 6131 (2013).

[44] Arunava Mukherjee, Shreya Shah, and Sukanta Bose, Observational constraints on spinning, relativistic Bose-Einstein condensate stars, Phys. Rev. D **91,** 084051 (2015).

[45] Nikolaos Stergioulas and John. L. Friedman, Comparing models of rapidly rotating relativistic stars constructed by two numerical methods, Astrophys. J. **444,** 306 (1995).

[46] Tiberiu Harko and Eniko J. M. Madarassy, Finite temperature effects in Bose-Einstein condensed dark matter halos, J. Cosmol. Astropart. Phys. 01 (2012) 020.

[47] Tiberiu Harko and Gabriela Mocanu, Cosmological evolution of finite temperature Bose-Einstein condensate dark matter, Phys. Rev. D **85,** 084012 (2012).

[48] S. Latifah, A. Sulaksono, and T. Mart, Boson star at finite temperature, Phys. Rev. D **90,** 127501 (2014).

[49] Christine Gruber and Axel Pelster, A theory of finite-temperature Bose-Einstein condensates in neutron stars, Eur. Phys. J. D **68,** 341 (2014).

[50] Gretel Quintero Angulo, Lismary de la Caridad Suárez González, Aurora Pérez Martínez, and Hugo Pérez Rojas, Effects of finite temperature on the magnetized equation of state in neutron stars composed of a Bose-Einstein condensate, Phys. Rev. C **108,** 015806 (2023).

[51] G. Ingrosso and R. Ruffini, On systems of self-gravitating bosons and fermions undergoing quantum condensation. Newtonian approach, Nuovo Cimento Soc. Ital. Fis. **101B,** 369 (1988).

[52] Neven Bilic and Hrvoje Nikolic, Self-gravitating bosons at nonzero temperature, Nucl. Phys. **B590,** 575 (2000).

[53] Jitesh R. Bhatt and V. Sreekanth, Boson stars: Chemical potential and quark condensates, arXiv:0910.1972.

[54] T. Matos and A. Suarez, Finite temperature and dissipative corrections to the Gross-Pitaevskii equation from $\lambda\Phi^4$ one loop contributions, Europhys. Lett. **96,** 56005 (2011).

[55] A. Griffin, Conserving and gapless approximations for an inhomogeneous Bose gas at finite temperatures, Phys. Rev. B **53,** 9341 (1996).

[56] E. Zaremba, T. Nikuni, and A. Griffin, Dynamics of trapped Bose gases at finite temperatures, J. Low Temp. Phys. **116,** 277 (1999).

[57] Allan Griffin, Tetsuro Nikuni, and Eugene Zaremba, *Bose-Condensed Gases at Finite Temperatures* (Cambridge University Press, New York, 2009).

[58] Richard C. Tolman, Static solutions of Einstein's field equations for spheres of fluid, Phys. Rev. **55,** 364 (1939).

[59] J. R. Oppenheimer and G. M. Volkoff, On massive neutron cores, Phys. Rev. **55,** 374 (1939).

[60] James B. Hartle, Slowly rotating relativistic stars. 1. Equations of structure, Astrophys. J. **150,** 1005 (1967).

[61] James B. Hartle and Kip S. Thorne, Slowly rotating relativistic stars. II. Models for neutron stars and supermassive stars, Astrophys. J. **153,** 807 (1968).

[62] Michi Bauböck, Emanuele Berti, Dimitrios Psaltis, and Feryal Özel, Relations between neutron-star parameters in the Hartle-Thorne approximation, Astrophys. J. **777,** 68 (2013).

[63] Enrico Barausse, Thomas P. Sotiriou, and Ian Vega, Slowly rotating black holes in Einstein-æther theory, Phys. Rev. D **93,** 044044 (2016).

[64] O. P. Jyothilakshmi, P. E. Sravan Krishnan, Prashant Thakur, V. Sreekanth, and T. K. Jha, Hyperon bulk viscosity and *r*-modes of neutron stars, Mon. Not. R. Astron. Soc. **516,** 3381 (2022).

[65] S. Chandrasekhar and E. A. Milne, The equilibrium of distorted polytropes: (I). The rotational problem, Mon. Not. R. Astron. Soc. **93,** 390 (1933).